Keratinocyte-specific *Smad2* ablation results in increased epithelial-mesenchymal transition during skin cancer formation and progression

Kristina E. Hoot,[1] Jessyka Lighthall,[2] Gangwen Han,[2] Shi-Long Lu,[2,3] Allen Li,[2] Wenjun Ju,[4] Molly Kulesz-Martin,[1,3] Erwin Bottinger,[4] and Xiao-Jing Wang[1,2,3]

[1]Department of Cell and Developmental Biology,
[2]Department of Otolaryngology, and [3]Department of Dermatology, Oregon Health & Science University, Portland, Oregon, USA.
[4]Department of Medicine, Mount Sinai School of Medicine, New York, New York, USA.

TGF-β and its signaling mediators, Smad2, -3, and -4, are involved with tumor suppression and promotion functions. *Smad4*$^{-/-}$ mouse epidermis develops spontaneous skin squamous cell carcinomas (SCCs), and *Smad3*$^{-/-}$ mice are resistant to carcinogen-induced skin cancer; however, the role of Smad2 in skin carcinogenesis has not been explored. In the present study, we found that Smad2 and Smad4, but not Smad3, were frequently lost in human SCCs. Mice with keratinocyte-specific *Smad2* deletion exhibited accelerated formation and malignant progression of chemically induced skin tumors compared with WT mice. Consistent with the loss of Smad2 in poorly differentiated human SCCs, *Smad2*$^{-/-}$ tumors were poorly differentiated and underwent epithelial-mesenchymal transition (EMT) prior to spontaneous Smad4 loss. Reduced E-cadherin and activation of its transcriptional repressor Snail were also found in *Smad2*$^{-/-}$ mouse epidermis and occurred more frequently in Smad2-negative human SCCs than in Smad2-positive SCCs. Knocking down Snail abrogated Smad2 loss–associated EMT, suggesting that Snail upregulation is a major mediator of Smad2 loss–associated EMT. Furthermore, Smad2 loss led to a significant increase in Smad4 binding to the Snail promoter, and knocking down either Smad3 or Smad4 in keratinocytes abrogated Smad2 loss–associated Snail overexpression. Our data suggest that enhanced Smad3/Smad4-mediated Snail transcription contributed to Smad2 loss–associated EMT during skin carcinogenesis.

Introduction

TGF-β signaling is involved in tissue homeostasis and cancer development (1). Ligand binding to heteromers of TGF-β type I and type II receptors (TGF-βRI and TGF-βRII) induces TGF-βRI to phosphorylate Smad2 and Smad3. Phosphorylated Smad2 and Smad3 bind a co-Smad, Smad4, and the heteromeric Smad complexes translocate into the nucleus to regulate transcription of TGF-β target genes (1). Smad3 binds to the Smad-binding element (SBE) of a target gene, and subsequently recruits Smad4 to the same SBE. Smad2 does not bind to DNA directly but complexes with Smad3 and Smad4 as either a coactivator or a corepressor for Smad3 and Smad4 (2). Each of these Smads has been implicated by in vitro studies in mediating the multiple functions of TGF-β (3). However, increasing numbers of studies show that Smad2, -3, and -4 are regulated differently and exhibit distinct physiological functions in vivo (2, 3). For instance, both *Smad2*- and *Smad4*-knockout mice are embryonic lethal due to failure in embryonic axis patterning and endoderm specification (4) and failure of proper endoderm and mesoderm formation (5), respectively. In contrast, *Smad3*-knockout mice are viable but succumb to mucosal immunity defects after birth (6).

In many cancer types, TGF-β signaling has a tumor suppressive effect early in carcinogenesis but promotes invasion and metastasis at later stages (7). Increasing evidence suggests that Smads mediate both tumor suppression and promotion functions of TGF-β. In epithelial cells, Smad2, -3, and -4 are involved in growth inhibition (2), a major tumor suppressive effect of TGF-β, and epithelial-mesenchymal transition (EMT) (8, 9), an early and major tumor promoting effect of TGF-β. However, genes associated with each of these biological processes are differentially regulated by individual Smads (1, 3). Loss of Smad2 or Smad4 at the genetic and protein levels has been widely reported in various cancer types (2, 10). In contrast, *Smad3* mutation is found only in colon cancer at a very low frequency (11), and Smad3 protein loss was reported only in pediatric T cell acute lymphoblastic leukemia (12). In human skin cancer, individual Smad expression patterns in squamous cell carcinomas (SCCs) have not been documented. The roles of individual Smads in skin carcinogenesis have been assessed mainly through genetically engineered mouse models. *Smad4* deletion in keratinocytes results in spontaneous SCC formation (13, 14), indicating a dominant tumor suppressive effect of Smad4 in skin carcinogenesis. *Smad3*-null keratinocytes transduced with a *v-ras* oncogene exhibited increased malignancy when grafted to immune-compromised mouse skin (15). However, *Smad3*-knockout mice are resistant to skin chemical carcinogenesis (16, 17) due to abrogation of TGF-β1-mediated inflammation and gene expression critical for tumor promotion (17). The role of Smad2 in skin carcinogenesis has not been fully explored in animal models as germline *Smad2*-knockout mice die in early embryogenesis (4). In the current study, we assessed the role and molecular mechanisms of Smad2 in skin carcinogenesis.

Nonstandard abbreviations used: DMBA, dimethylbenz[α]anthracene; EMT, epithelial-mesenchymal transition; IHC, immunohistochemistry; K5, keratin 5; *K5.Cre*PR1*, mutant Cre recombinase fused to a truncated progesterone receptor targeted by K5 promoter; LOH, loss of heterozygosity; qRT-PCR, quantitative RT-PCR; SBE, Smad-binding element; SCC, squamous cell carcinoma; TPA, 12-*O*-tetradecanoyl-phorbol-13-acetate.

Conflict of interest: The authors have declared that no conflict of interest exists.

Citation for this article: *J. Clin. Invest.* **118**:2722–2732 (2008). doi:10.1172/JCI33713.

Table 1
Proteins of Smad2 and Smad4, but not Smad3, were lost in human skin SCCs

	Smad2 loss	Smad3 loss	Smad4 loss
Total Smad loss/Total skin SCC samples	58/83	4/83	58/83
Well-differentiated loss	5/30[A]	1/30	14/30
Poorly differentiated loss	53/53[B,C]	3/53	44/53[B]

The number of SCC cases with individual Smad protein loss compared with the total number of SCC cases. Both Smad2 and Smad4 loss occurred at higher rates in poorly differentiated SCCs versus in well-differentiated SCCs. However, Smad2 loss was more closely correlated with poorly differentiated SCCs than Smad4 loss. [A]$P = 0.025$; [B]$P < 0.001$ compared poorly differentiated SCCs to well-differentiated SCCs; [C]$P = 0.005$ compared cases with Smad2 loss to cases with Smad4 loss.

Results

Smad2 and Smad4 were frequently lost in human skin SCCs. We examined Smad2 expression patterns by immunohistochemistry (IHC) in 83 human skin SCCs. Smad3, a Smad2 signaling partner, and co-Smad, Smad4, were also examined. In comparison with the epidermis in normal skin, Smad2 and Smad4 each were lost in 70% of skin SCC samples, whereas Smad3 loss was only seen in 5% of cases (Table 1 and Supplemental Figure 1; supplemental material available online with this article; doi:10.1172/JCI33713DS1). Additionally, the incidence of Smad2 loss occurred in 100% of poorly differentiated SCCs, which was significantly higher than Smad4 loss in poorly differentiated SCCs ($P = 0.005$; Table 1).

To determine whether loss of Smad2 and Smad4 proteins in human skin cancer occurs at the pretranslational level, we examined mRNA levels of *Smad2* and *Smad4* from 33 cases of poorly differentiated human SCCs and 6 normal skin samples. In comparison with control skin, 31/33 (94%) of human skin SCC samples showed at least a 50% reduction of *Smad2* mRNA, and 28/33 (85%) of these samples showed at least a 50% reduction of *Smad4* mRNA (Figure 1A). Such high rates of *Smad2* and *Smad4* loss at the mRNA level prompted us to examine if they are lost at the genetic level. Among samples with more than 50% mRNA reduction of *Smad2* and *Smad4*, 21 samples contained adjacent nonneoplastic skin in their paraffin sections. We dissected the adjacent nonneoplastic skin in each section as a control for each tumor sample and performed a loss of heterozygosity (LOH) analysis for *Smad2* and *Smad4* (Figure 1B and Supplemental Figure 2). We found that 14 samples (67%) exhibited LOH at the *Smad2* locus, and 12 samples (57%) exhibited LOH at the *Smad4* locus. A total of 17 samples (81%) had LOH at either the *Smad2* or *Smad4* locus.

Keratinocyte-specific Smad2 deletion resulted in increased susceptibility to skin carcinogenesis. Our previous study has revealed that Smad4 loss in keratinocytes results in spontaneous skin SCCs (14). To determine if the high incidence of Smad2 loss in human skin SCCs also plays a causal role in skin carcinogenesis, we generated keratinocyte-specific *Smad2*-knockout mice (Supplemental Figure 3). Mice with RU486-controlled Cre recombinase targeted by a keratin 5 (K5) promoter (*K5.Cre*PR1*) were generated as previously reported (18). We mated *K5.Cre*PR1* mice with *Smad2* floxed mice ($Smad2^{f/f}$) (19). *Smad2* deletion in keratinocytes was achieved by topical application of RU486. Unlike $Smad4^{-/-}$ epidermis, $Smad2^{-/-}$ mice did not develop spontaneous tumors within 18 months. To further assess whether Smad2 loss alters susceptibility to skin carcinogen-

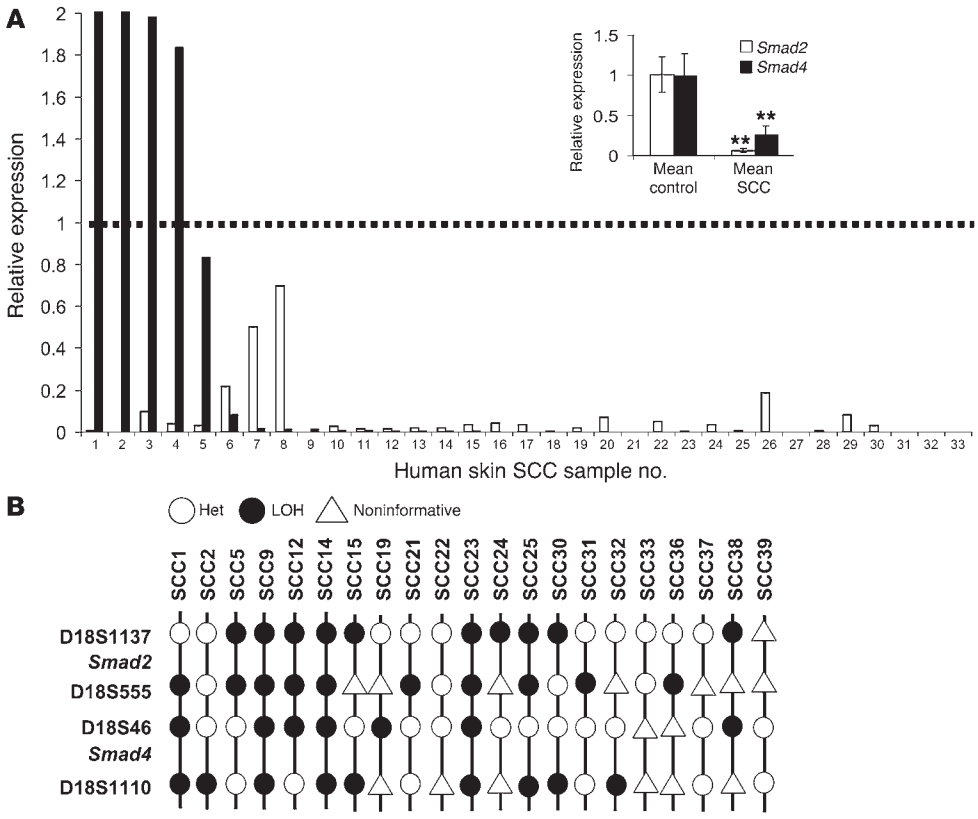

Figure 1
Reduced mRNA and LOH of *Smad2* and *Smad4* in human skin SCCs. (**A**) qRT-PCR of 33 human skin SCCs showed loss of *Smad2* (31/33 samples) and *Smad4* (28/33 samples) expression compared with normal skin controls. The inset shows the mean value for control and skin SCC. $^{**}P < 0.001$. (**B**) LOH of *Smad2* and *Smad4* in human SCCs. Microsatellite markers D18S1137 and D18S555 were used to assess *Smad2* LOH, and D18S46 and D18S1110 were used to assess *Smad4* LOH. Het, heterozygosity; Noninformative, adjacent tissue exhibited homozygosity.

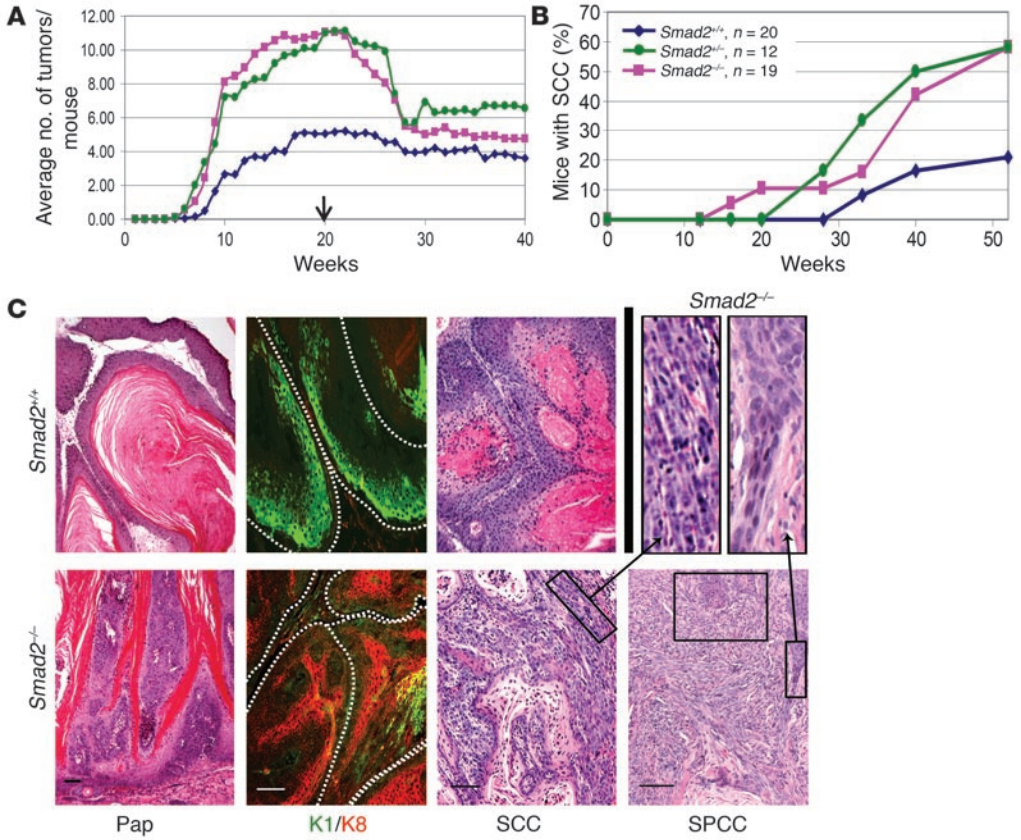

Figure 2

Accelerated tumor formation and malignant conversion of skin carcinogenesis in *K5.Smad2*-knockout mice. (**A**) Kinetics of tumor formation. Arrow indicates TPA withdrawal. The seemingly more rapid tumor regression after TPA withdrawal in *Smad2*$^{+/-}$ and *Smad2*$^{-/-}$ groups compared with *Smad2*$^{+/+}$ is due to necessity of euthanizing mice with a higher tumor burden. $P < 0.001$ compared with *K5.Smad2*$^{-/-}$ or *K5.Smad2*$^{+/-}$ and *Smad2*$^{+/+}$ (**B**) Kinetics of malignant conversion. *Smad2*$^{+/-}$ and *Smad2*$^{-/-}$ mice had higher rates of malignant conversion ($P < 0.05$ compared with *Smad2*$^{+/+}$ mice). The total number of mice of each genotype was used as a denominator for all time points through the entire course of tumor kinetics in **A** and **B**. (**C**) Tumor pathology and keratin markers. H&E staining of *K5.Smad2*$^{-/-}$ tumors showed less differentiation compared with *K5.Smad2*$^{+/+}$ tumors. Immunofluorescence staining revealed that at the same histological stage, *Smad2*$^{+/+}$ papillomas (Paps) expressed K1 (green) in suprabasal layers, whereas *K5.Smad2*$^{-/-}$ papillomas expressed K8 (red) and almost lost K1 in suprabasal layers. The dotted lines delineate the basement membrane. At SCC stages, *K5.Smad2*$^{-/-}$ tumors developed spindle cell carcinomas (SPCCs) when *K5.Smad2*$^{+/+}$ tumors were well-differentiated SCCs. Rectangles in the bottom 2 panels denote areas of transition from SCC to SPCC. Two of these regions are enlarged 4 times to illustrate this transition (top row, far right panels). Scale bars: 100 μm.

esis, we applied a 2-stage chemical carcinogenesis protocol, which gives discrete stages of benign papillomas and malignant SCCs in normal mice (17). Littermates from *K5.Cre*PR1* and *Smad2*$^{f/f}$ breeding were divided by their genotypes (*K5.Cre*PR1/Smad2*$^{f/f}$ for *K5.Smad2*$^{-/-}$; *K5.Cre*PR1/Smad2*$^{f/wt}$ for *K5.Smad2*$^{+/-}$; *K5.Cre*PR1*, *Smad2*$^{f/f}$, and *Smad2*$^{f/wt}$ for *Smad2*$^{+/+}$) and treated with 20 μg RU486 daily for 5 days at 6 weeks of age to induce *Smad2* gene deletion in keratinocytes. Two weeks after RU486 treatment, when keratinocytes in the entire epidermis were expected to be replaced with *Smad2*$^{-/-}$ or *Smad2*$^{+/-}$ epidermal stem cells in *K5.Cre*PR1/Smad2*$^{f/f}$ or *K5.Cre*PR1/Smad2*$^{f/wt}$ mice, respectively, we topically applied a subcarcinogenic dose of dimethylbenz[α]anthracene (DMBA, 20 μg/mouse). One week later, we began to topically apply 12-*O*-tetradecanoyl-phorbol-13-acetate (TPA, 5 μg/mouse) twice a week for 20 weeks. *K5.Smad2*$^{-/-}$ and *K5.Smad2*$^{+/-}$ mice developed tumors faster and had 2- to 3-fold more tumors per mouse than *Smad2*$^{+/+}$ mice ($P < 0.001$; Figure 2A). Malignant conversion was also accelerated in *K5.Smad2*$^{-/-}$ and *K5.Smad2*$^{+/-}$ mice ($P < 0.05$ compared with *Smad2*$^{+/+}$ mice). Notably, at each time point, more *K5.Smad2*$^{-/-}$ and *K5.Smad2*$^{+/-}$ mice developed SCCs than *Smad2*$^{+/+}$ mice (Figure 2B). These results indicate Smad2-deficient epidermis is more susceptible to skin tumor formation and malignant conversion.

Because *K5.Smad2*$^{+/-}$ also exhibited accelerated tumor formation and malignant progression similar to *K5.Smad2*$^{-/-}$ mice, we examined endogenous Smad2 levels in *K5.Smad2*$^{+/-}$ tumors. Smad2 protein was still detectable in all *K5.Smad2*$^{+/-}$ papillomas but was lost in 60% cases of *K5.Smad2*$^{+/-}$ SCCs (Supplemental Figure 4). At this stage, approximately 45% SCC cases from *Smad2*$^{+/+}$ mice also lost Smad2 protein as determined by Smad2 antibody staining (Supplemental Figure 4; $P < 0.05$). These data suggest haploid insufficiency of *Smad2*$^{+/-}$ keratinocytes at early stages of skin carcinogenesis, and spontaneous Smad2 protein loss from the remaining allele in SCCs caused them to progress to malignancy, similar to *Smad2*$^{-/-}$ SCCs.

K5.Smad2$^{-/-}$ *tumors were poorly differentiated and exhibited an increase in EMT.* To determine whether accelerated skin carcinogen-

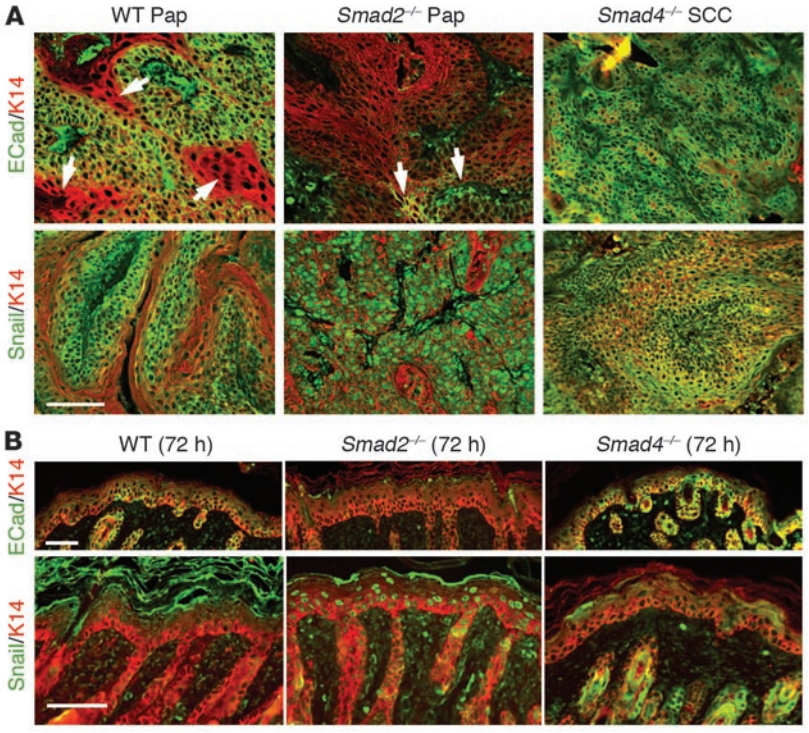

Figure 3
Snail activation and E-cadherin (ECad) loss in *K5.Smad2*$^{-/-}$ tissues. A K14 antibody was used for counterstain (red). (**A**) *K5.Smad2*$^{-/-}$ papillomas undergo EMT. When most of cells in *Smad2*$^{+/+}$ papillomas or spontaneous *Smad4*$^{-/-}$ SCCs still retained E-cadherin staining (green), *K5.Smad2*$^{-/-}$ papillomas show significant loss of E-cadherin (green). Arrows in *K5.Smad2*$^{+/+}$ image indicate patchy areas of E-cadherin loss, whereas arrows in *K5.Smad2*$^{-/-}$ tumors show patchy retention of E-cadherin (top row). At this stage, Snail staining (green) was primarily cytoplasmic in *Smad2*$^{+/+}$ papillomas and spontaneous *Smad4*$^{-/-}$ SCCs, but *K5.Smad2*$^{-/-}$ tumors displayed nuclear Snail staining (bottom row). Scale bar: 100 μm. (**B**) *K5.Smad2*$^{-/-}$ pup skin 72 hours after *Smad2* deletion demonstrated significant reduction of E-cadherin (green, upper row) with a concomitant increase in nuclear Snail (green, bottom row). *K5.Smad4*$^{-/-}$ pup skin 72 hours after *Smad4* deletion showed no change in E-cadherin and Snail expression patterns from WT skin. Scale bar: 100 μm.

esis in *K5.Smad2*$^{-/-}$ mice was a result of abrogating TGF-β-induced growth inhibition and/or apoptosis, we evaluated cell proliferation via BrdU incorporation and apoptosis via the TUNEL assay. Apoptosis in *K5.Smad2*$^{-/-}$ nonlesional and tumor tissues did not differ from those in *K5.Smad2*$^{+/+}$ controls (data not shown). Although nonlesional *K5.Smad2*$^{-/-}$ skin did not show increased proliferation, TPA-treated *K5.Smad2*$^{-/-}$ skin exhibited increased proliferation and epidermal hyperplasia (Supplemental Figure 5). However, proliferation rates became comparable in tumors between *K5.Smad2*$^{-/-}$ and WT mice (data not shown). Histological analyses revealed that *K5.Smad2*$^{-/-}$ tumors were generally poorly differentiated. The earliest *K5.Smad2*$^{-/-}$ papillomas lacked stratified epithelial structure (Figure 2C) and exhibited loss of loricrin and filaggrin, which are terminal differentiation markers (data not shown), and K1, an early differentiation marker (Figure 2C), but expressed K8 (Figure 2C), a marker of simple epithelia that is not expressed in stratified epithelia but is usually expressed in late-stage SCCs (20). In contrast, papillomas in WT mice showed partial or complete loss of loricrin and filaggrin (data not shown), without K8 expression, but retained uniform K1 expression (Figure 2C). At the SCC stage, *K5.Smad2*$^{-/-}$ SCCs were poorly differentiated and often showed clusters of cells that underwent EMT (Figure 2C), whereas most SCCs from WT mice were well differentiated (Figure 2C). While only 1 out of 20 WT mice developed an EMT-type of spindle cell carcinoma (SPCC) 50 weeks after TPA promotion, *K5.Smad2*$^{+/-}$ and *K5.Smad2*$^{-/-}$ mice developed more SPCCs at earlier time points (3 out of 12 *K5.Smad2*$^{+/-}$ and 5 out of 19 *K5.Smad2*$^{-/-}$ starting at 27–35 weeks).

K5.Smad2$^{-/-}$ *tumors exhibited pathological alterations associated with EMT.* The poorly differentiated nature of *Smad2*$^{-/-}$ tumors prompted us to examine the status of E-cadherin, an adhesion molecule critical for maintaining epithelial structure. While E-cadherin was lost in only patchy areas of late-stage *Smad2*$^{+/+}$ papillomas, *Smad2*$^{-/-}$ papillomas exhibited nearly complete loss of E-cadherin (Figure 3). In contrast, early stage *Smad4*$^{-/-}$ spontaneous SCCs retained membrane-associated E-cadherin in most tumor cells (Figure 3). We then examined expression patterns of Snail, a transcriptional repressor of E-cadherin (21). Snail antibody staining, which recognizes both Snail and Slug, revealed a patchy, cytoplasmic staining pattern in WT papillomas and early stage *Smad4*$^{-/-}$ spontaneous SCCs (Figure 3). In contrast, *Smad2*$^{-/-}$ tumors exhibited strong Snail staining primarily in the nucleus (Figure 3). Both chemically induced WT SCCs and *Smad4*$^{-/-}$ spontaneous SCCs showed reduced E-cadherin and increased Snail nuclear staining in late stages, approximately 10–20 weeks after SCC formation (data not shown). *K5.Smad2*$^{-/-}$ tumors also showed an increase in mesenchymal markers, vimentin and αSMA (Supplemental Figure 6A), which are associated with motility and invasiveness (22, 23). These markers were restricted to the stroma of *K5.Smad2*$^{+/+}$ papillomas and spontaneous *Smad4*$^{-/-}$ SCCs but were detected in both tumor epithelia and stroma of *K5.Smad2*$^{-/-}$ papillomas. Additionally, vimentin and αSMA were present in the hyperplastic epidermis adjacent to papillomas of *K5.Smad2*$^{-/-}$ mice (Supplemental Figure 6B), suggesting that EMT is a relatively early event in *K5.Smad2*$^{-/-}$ carcinogenesis. We then examined if the EMT phenotype occurs in *K5.Smad2*$^{-/-}$ without exposure to a carcinogen. Seventy-two hours after Smad2 was deleted in neonatal skin, a marked loss of E-cadherin and an associated increase in nuclear Snail were seen in *Smad2*$^{-/-}$ epidermis and hair follicles when compared with RU486-treated WT and *K5.Smad4*$^{-/-}$ skin (Figure 3B). However, vimentin and αSMA were not detected in *K5.Smad2*$^{-/-}$ epidermis (data not shown). These results suggest that EMT is an early effect of Smad2 loss, and additional insults during carcinogenesis further enhanced Smad2 loss–associated EMT phenotype.

Smad2 loss resulted in molecular alterations of TGF-β target genes associated with EMT. To assess if Smad2 loss–associated EMT was associ-

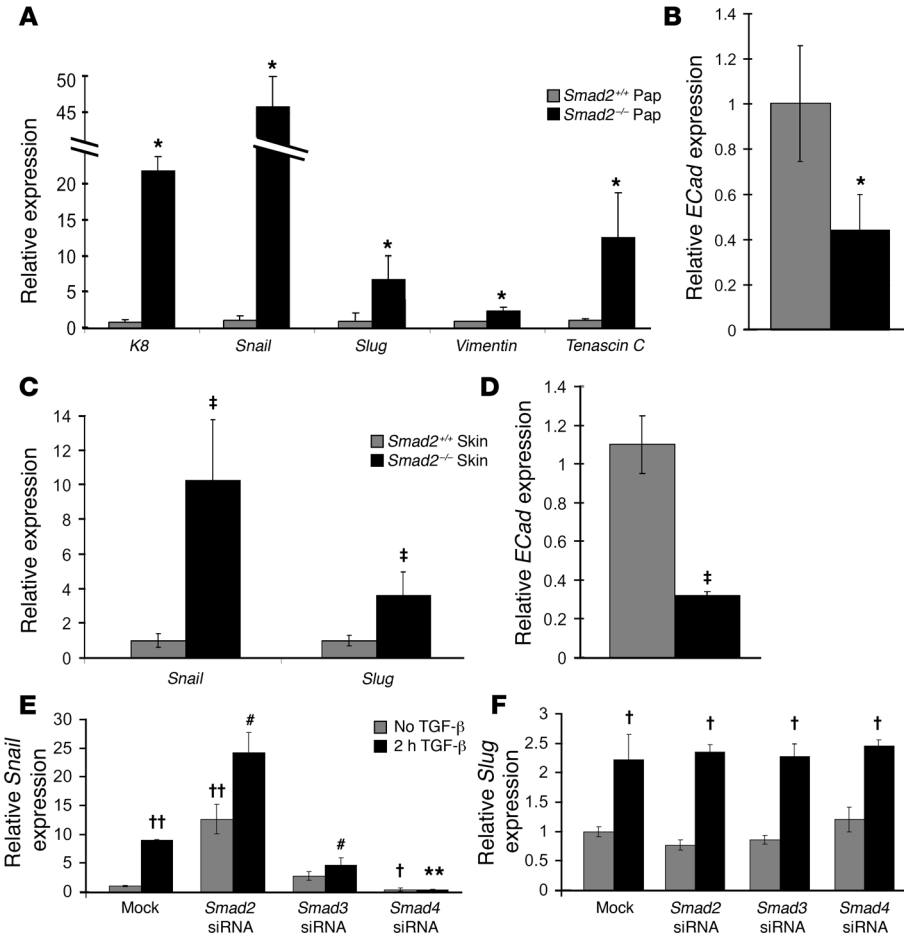

Figure 4
Altered gene expression associated with dedifferentiation and EMT in *K5.Smad2*$^{-/-}$ papillomas and epidermis. (**A**) Upregulated mRNA expression of K8- and EMT-associated molecules in *K5.Smad2*$^{-/-}$ papillomas. *$P < 0.05$ compared with *Smad2*$^{+/+}$ papillomas. (**B**) Downregulation of E-cadherin in *K5.Smad2*$^{-/-}$ papillomas. All changes in *Smad2*$^{-/-}$ papillomas are statistically significant in comparison with *Smad2*$^{+/+}$ papillomas. *$P < 0.05$ compared with *Smad2*$^{+/+}$ papillomas. (**C**) Upregulation of *Snail* and *Slug* mRNA in *K5.Smad2*$^{-/-}$ epidermis. ‡$P < 0.01$ compared with WT skin. (**D**) Downregulation of E-cadherin in *K5.Smad2*$^{-/-}$ epidermis. ‡$P < 0.01$ compared with WT skin. (**E**) *Snail* expression levels after knocking down individual Smads in HaCaT cells. #$P < 0.05$ compared with mock transfection treatment with TGF-β1. **$P < 0.001$ compared with mock transfection with TGF-β1 treatment. ††$P < 0.001$ compared with mock transfection without TGF-β1. †$P < 0.05$ compared with mock transfection without TGF-β1 (**F**) *Slug* expression levels after knocking down individual Smads in HaCaT cells. †$P < 0.05$ compared with mock transfection without TGF-β1.

ated with increased TGF-β1 ligand, which plays an important role in EMT (24), we examined TGF-β1 levels in WT and *Smad2*$^{-/-}$ skin and tumors. We found neither elevated TGF-β1 nor alterations of Smad3 and Smad4 in *K5.Smad2*$^{-/-}$ skin and papillomas in comparison with WT controls (data not shown). Elevated TGF-β1 protein was found in WT and *K5.Smad2*$^{-/-}$ SCCs at comparable levels (Supplemental Figure 7). Consistent with this data, western analyses showed that in comparison with WT tumors, *K5.Smad2*$^{-/-}$ tumors did not have increased levels of pJNK, pERK, and pMAPK (data not shown), the major non-Smad pathways of TGF-β–induced EMT that require a higher level of TGF-β1 than that found in WT tumors (25). Consistent with our previous observation that approximately 30%–40% of chemically induced SCC cases exhibited reduction in Smad3 and Smad4 at late stages (26), both WT and *K5.Smad2*$^{-/-}$ SCCs showed reduced Smad3 and Smad4 in approximately 40% of cases (data not shown). SCCs that retained Smad3 showed similar patterns between WT and *K5.Smad2*$^{-/-}$ mice (Supplemental Figure 7). *K5.Smad2*$^{-/-}$ SCCs that retained Smad4 showed more nuclear staining than *K5.Smad2*$^{+/+}$ SCCs (Supplemental Figure 7). To further determine whether changes in EMT-associated proteins are the result of transcriptional deregulation of these genes by Smad2 loss, we examined mRNA levels of these molecules in *K5.Smad2*$^{-/-}$ and *K5.Smad2*$^{+/+}$ papillomas, at the stage prior to the pathological appearance of EMT cells in *K5.Smad2*$^{-/-}$ tumors. Transcripts of K8, Snail, Slug, vimentin, and tenascin C were all significantly upregulated in *K5.Smad2*$^{-/-}$ papillomas in comparison with WT papillomas (Figure 4A). In contrast, transcripts of E-cadherin were downregulated in *Smad2*$^{-/-}$ papillomas in comparison with WT controls (Figure 4B). Further, increased transcripts of Snail and Slug and decreased E-cadherin transcripts were also detected in day 3 *K5.Smad2*$^{-/-}$ skin in comparison with WT skin (Figure 4, C and D). No changes in expression levels of vimentin and tenascin C were observed in *K5.Smad2*$^{-/-}$ skin (data not shown). These data suggest that upregulation of Snail and/or Slug and the subsequent E-cadherin reduction represent an early effect of Smad2 loss in keratinocytes.

To assess if Smad2 regulates Snail and Slug differently from Smad3 and Smad4 in keratinocytes, we examined expression levels of Snail and Slug in cultured human HaCaT keratinocytes after knocking down Smad2, -3, or -4. After 48 to 72 hours of transfection of HaCaT cells with siRNAs for Smad2, -3, or -4, the respective mRNA levels were reduced by at least 70% (Supplemental Figure 8). In mock-transfected cells, increased *Snail* mRNA was detected after 1 hour of TGF-β1 treatment and remained increased for 48 hours (data not shown), with a 9-fold increase at 2 hours (Figure 4E). After Smad2 was knocked down for 72 hours, Snail expression was increased by 13-fold, and further increased by 24-fold after 2 hours TGF-β1 treatment (Figure 4E). In contrast, knockdown of Smad3 did not affect baseline Snail expression but significantly attenuated TGF-β1–induced Snail expression (Figure 4E). Knocking down Smad4 abrogated both baseline and TGF-β1–induced Snail expression (Figure 4E). Slug expression was also induced by

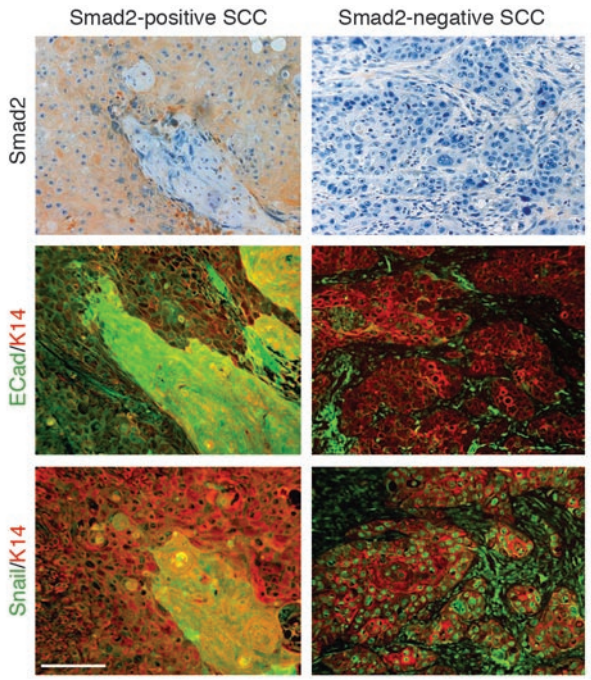

Figure 5
Human skin SCCs with Smad2 loss correlated with E-cadherin loss and nuclear Snail. Skin SCCs were stained for Smad2 IHC (brown, top row), and immunofluorescence staining was performed for E-cadherin (green; middle row) and Snail (green; bottom row). A K14 antibody was used for immunofluorescent counterstain (red). An example of a pair SCCs from serial sections showed that a Smad2-positive SCC retained membrane-associated E-cadherin with a few Snail nuclear staining cells. In contrast, SCC with Smad2 loss lost membrane-associated E-cadherin but uniformly expressed Snail in the nucleus. Scale bar: 100 μm.

TGF-β1 treatment, with a 2-fold increase 2 hours after TGF-β1 treatment (Figure 4F). However, none of the individual Smads affected Slug expression levels, with or without TGF-β1 treatment (Figure 4F). These data suggest that expression of Snail, but not Slug, is regulated by Smads. Thus, in vivo Slug overexpression in *K5.Smad2*$^{-/-}$ keratinocytes could be a secondary event.

Next, we assessed if Smad2 loss correlated to Snail overexpression in human skin SCCs. Overall, Snail overexpression and E-cadherin loss occurred at high frequencies in human skin SCCs. However, consistent with the association of Smad2 loss with poorly differentiated SCCs (Table 1), Smad2-negative SCCs (52 cases) exhibited a higher incidence of Snail overexpression than in 23 cases of Smad2-positive SCCs (90% vs. 73%; $P < 0.05$; Figure 5). Similarly, the rate of E-cadherin loss occurred in 79% of Smad2-negative SCCs versus 60% in Smad2-positive SCCs ($P < 0.05$; Figure 5).

Elevated Snail contributed markedly to Smad2 loss–associated EMT. Since the data from *K5.Smad2*$^{-/-}$ mice, human keratinocytes, and human skin SCCs revealed a correlation between Snail overexpression and Smad2 loss, we assessed whether increased Snail expression functionally contributed to Smad2 loss–associated EMT by knocking down Snail together with Smad2 in HaCaT cells (Figure 6). In control keratinocytes, sporadic Snail nuclear staining cells were detected and E-cadherin stained the cell membrane. After 72 hours of Snail knockdown, Snail expression and protein was reduced by 80% (Supplemental Figure 8), and the number of Snail nuclear positive cells was markedly reduced (Figure 6). E-cadherin staining in Snail siRNA–treated cells retained a similar pattern to control cells. After 72 hours of Smad2 knockdown, HaCaT cells lost the typical keratinocyte appearance, and some of them exhibited fibroblast-like morphology (Figure 6), which correlated with increased Snail nuclear staining and loss of membrane-associated E-cadherin (Figure 6). However, knocking down both Smad2 and Snail restored membrane-associated E-cadherin staining and epithelial morphology (Figure 6), suggesting that Snail is the major target of Smad2 loss and contributes to Smad2 loss–associated EMT.

Enhanced Smad4 binding to the Snail promoter in Smad2-deficient keratinocytes. To further analyze whether Snail overexpression induced by Smad2 loss was the result of enhanced transcriptional activity of Smad3 and/or Smad4, we performed in vivo chromatin immunoprecipitation (ChIP) for Smad binding to the Snail promoter in neonatal WT and *Smad2*$^{-/-}$ mouse skin. Within the TGF-β–regulatory region of the mouse Snail promoter, as identified by previous studies (9, 27), there are 2 SBEs at –438 bp and –1,077 bp upstream of the *Snail* transcriptional start site (TSS). We found that in WT skin, Smad2, -3, and -4 bound to both sites (Figure 7, A and B) but not to intronic regions of the gene (data not shown). Quantitative PCR on the precipitated chromatin revealed that in *Smad2*$^{-/-}$ skin, Smad3 binding to both SBEs was at a capacity similar to that in WT skin (Figure 7, A and B), suggesting that Smad2 does not affect the affinity of Smad3 binding to the Snail promoter. However, Smad4 binding to the Snail promoter increased by 8- and 29-fold on the –438-bp and the –1,077-bp sites, respectively, in *K5.Smad2*$^{-/-}$ skin compared with that in WT skin (Figure 7, A and B). Therefore, these data suggest that normally, Smad2 either competes with, or impedes Smad4 binding to the SBE at the Smad3-binding site on the Snail promoter. To further assess if Smad2 loss–associated increase in Smad4 binding to the Snail promoter contributes to Snail overexpression, we knocked down Smad4 together with knockdown of Smad2. Knocking down Smad4 abrogated Smad2 loss–associated Snail overexpression (Figure 7C), suggesting that increased Smad4 binding contributed to transcriptional regulation of Snail in *K5.Smad2*$^{-/-}$ keratinocytes. Knockdown of Smad3 also abrogated Smad2 loss–associated Snail overexpression, suggesting that Smad3 binding in a complex with Smad4 is required for increased Snail transcription in Smad2-deficient keratinocytes.

Discussion

Smad2 and Smad4, but not Smad3, are frequently lost in human skin SCCs. In the current study, we found that proteins of Smad2 or Smad4, but not Smad3, were frequently lost in human skin SCCs. In cases with LOH of *Smad2* or *Smad4*, single-copy genetic loss may contribute to at least 50% loss of their transcripts and protein in each case, as mice with heterozygous deletion of *Smad2* or *Smad4* exhibited ~50% loss of transcripts and protein of these 2 molecules (see also ref. 28). Additionally, transcriptional and post-translational modifications could contribute to further loss of the remaining Smad2 and Smad4 transcripts and protein. Several Smad ubiquitin-E3 ligases, which contribute to Smad protein degradation, have been identified, some of which have been shown to be overexpressed in cancer (29–32). Thus, multiple mechanisms from the genetic to the posttranslational level could explain loss of Smad2 and Smad4 proteins, which are among the most frequent molecular alterations in skin cancer. Indeed, Smad2 and Smad4

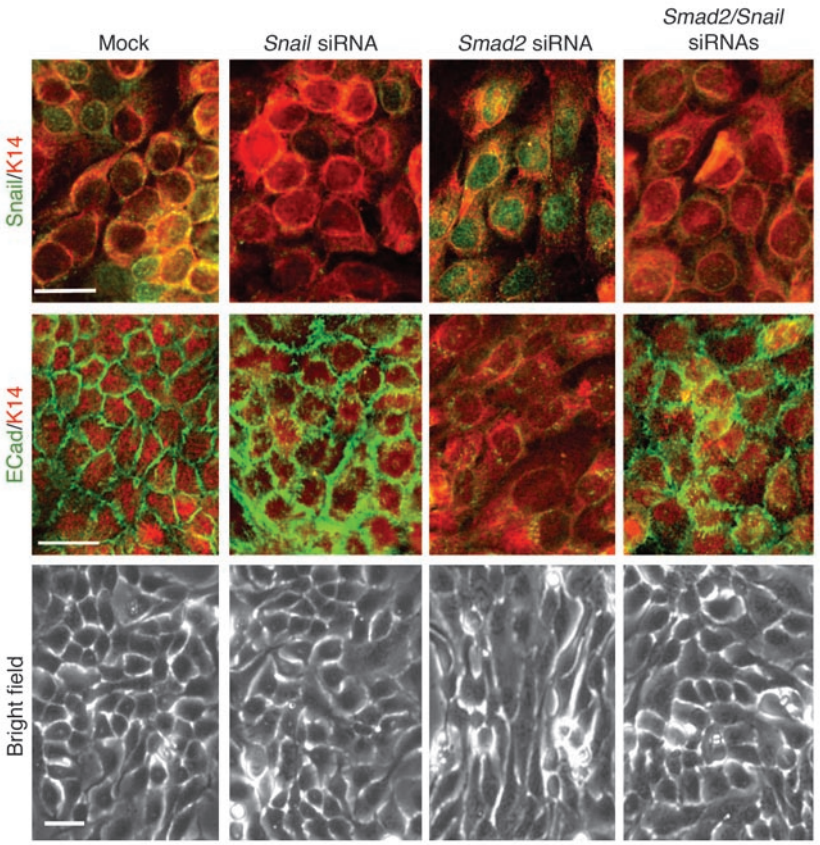

Figure 6
Snail contributed to Smad2 loss–associated EMT. *Smad2* knockdown caused an increase in Snail nuclear staining (green) compared with mock transfection and loss of E-cadherin (green) membrane staining, with more spindle-like morphology in HaCaT keratinocytes. A K14 antibody was used for counterstain (red). Remaining Snail staining in Snail siRNA transfected cells could be due to antibody cross reaction with Slug. E-cadherin staining had a pattern similar to mock control. *Smad2* and Snail concomitant knockdown resulted in reduced Snail staining in comparison with *Smad2* siRNA transfected cells and restoration of membrane E-cadherin staining. Phase contrast photos show epithelial morphology of the mock-transfected or Snail siRNA–transfected cells. Epithelial morphology was lost in *Smad2* siRNA–transfected cells, but was restored by cotransfection with Snail siRNA. Scale bar: 20 μm.

loss occurs more frequently than the currently known common molecular alterations in human skin SCCs, e.g., oncogene ras activation or loss of the p53 tumor suppressor (33). Notably, the incidences of Smad2 and Smad4 loss in skin SCCs found in this study are much higher than in head and neck SCCs (34). These differences may reflect cancer etiology, which is largely attributed to UV irradiation in skin cancer and to tobacco carcinogen exposure in head and neck cancer.

Smad2 has a tumor suppressive effect on the skin. Unlike keratinocyte-specific *Smad4*-knockout mice, which developed spontaneous skin SCCs, *K5.Smad2*$^{-/-}$ mice developed skin tumors neither spontaneously nor with TPA treatment alone (without DMBA initiation, data not shown), even though *K5.Smad2*$^{-/-}$ epidermis exhibited an increase in proliferation in response to TPA application. Thus, the increased proliferative potential of *K5.Smad2*$^{-/-}$ epidermis is insufficient as an initiator for skin carcinogenesis. This result is consistent with Smad2 expression patterns in human skin SCCs, in which Smad2 loss occurs only in SCCs but not in early stage actinic keratosis (25). Conversely, in the presence of a DMBA-induced H-ras mutation, a genetic alteration mimicking early stage human skin cancer (35), *K5.Smad2*$^{-/-}$ mice still did not develop skin tumors without TPA promotion (data not shown). Thus, Smad2 loss alone is also insufficient to promote initiated cells for cancer development. However, with both DMBA initiation and TPA promotion, *K5.Smad2*$^{-/-}$ mice were more susceptible to skin tumor formation and malignant conversion than WT mice. Although the current study limits the assessment of the true malignant conversion rate for each papilloma due to the necessity of euthanizing SCC-bearing mice with multiple papillomas, more *K5.Smad2*$^{-/-}$ mice developed SCCs at the same time points when compared with WT mice. Additionally, *K5.Smad2*$^{-/-}$ papillomas already harbored molecular changes seen in WT SCCs but not in papillomas, suggesting that the malignant progression program was in place prior to the pathological progression in *K5.Smad2*$^{-/-}$ tumors. Thus, Smad2 loss appears to cooperate with other molecular alterations elicited by the chemical carcinogenesis protocol to promote skin carcinogenesis. Interestingly, *K5.Smad2*$^{+/-}$ mice displayed tumor kinetics similar to *K5.Smad2*$^{-/-}$ mice. This observation is also consistent with a previous report that germline *Smad2* heterozygous mice exhibited accelerated tumor formation and malignant progression in a skin chemical carcinogenesis experiment (16). These studies suggest a haploid insufficiency for *Smad2* in tumor suppression.

Smad2 loss triggers molecular and pathological alterations associated with EMT. Our current study reveals that in human skin cancer, Smad2 loss was associated with dedifferentiation, loss of E-cadherin, and Snail activation. Correlated with this observation, the accompanying animal study reveals that loss of Smad2 triggers pathological and molecular alterations associated with dedifferentiation and EMT started in nonlesional *Smad2*$^{-/-}$ epidermis. Among EMT associated genes, Snail overexpression appears to be a major target and mediator of Smad2 loss-induced EMT.

The effect of Smad2 loss on EMT is somewhat surprising given that TGF-β signaling is well documented to promote EMT via both Smad and non-Smad pathways (24). Unlike keratinocytes with knockdown of TGF-βRII, which overexpress TGF-β1 (25, 36), Smad2 loss did not cause increased TGF-β1. However, our data revealed a significant increase in promoter binding of Smad4 to the Snail promoter in *Smad2*$^{-/-}$ keratinocytes. It is possible that

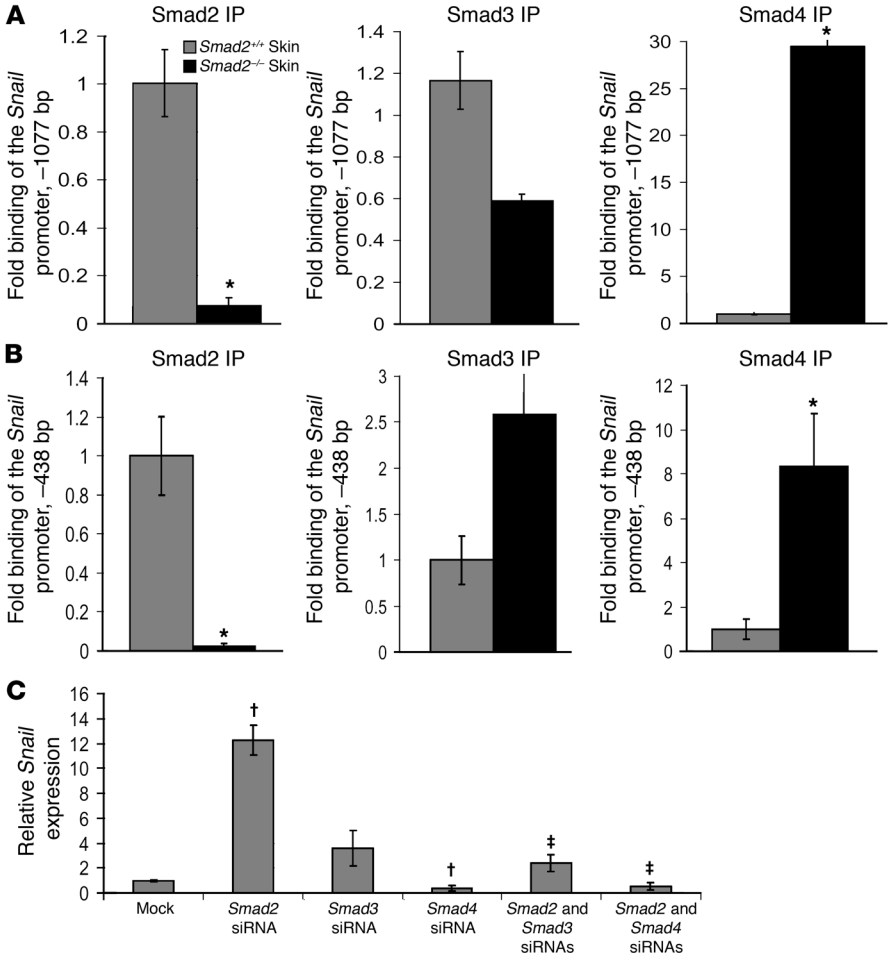

Figure 7
Increased Smad3/Smad4-mediated Snail transcription contributes to Smad2 loss–associated Snail overexpression. (**A** and **B**) Comparative PCR from chromatin immunoprecipitation (IP) showed an increase in Smad4 binding to the Snail promoter in *Smad2*$^{-/-}$ skin compared with WT skin. Residue Smad2 binding in *Smad2*$^{-/-}$ skin was from nonkeratinocyte population of the whole skin. Smad3 binding to the Snail promoter was not significantly changed in *Smad2*$^{-/-}$ skin in comparison with WT skin. Smad4 binding to the Snail promoter was significantly increased in *Smad2*$^{-/-}$ skin. *$P < 0.05$. (**C**) Dual knockdown of *Smad2* and *Smad3* or *Smad2* and *Smad4* abrogated *Smad2* loss–associated Snail overexpression. *Smad2* knockdown (48 hours) caused a significant increase in Snail expression. Knockdown of *Smad4* alone caused a reduction in Snail expression. Concomitant knockdown of *Smad2* and *Smad3* or *Smad2* and *Smad4* reduced Snail expression back to mock-transfection levels. †$P < 0.05$ compared with mock transfection. ‡$P < 0.05$ compared with *Smad2* siRNA treatment.

normally Smad2 either competes with or impedes the ability of Smad4 to bind Smad3 on the SBEs of the Snail promoter, therefore Smad2 loss confers more binding of Smad4 with Smad3. Although Smad2 has been shown to activate Snail, it is likely that Smad2 has a much weaker effect than Smad4, given the fact that Smad2, but not Smad4, normally recruits transcriptional corepressors to SBEs (2). Based on this, once Smad2 is lost, the corepressors would not be recruited to the SBEs, and Smad3 together with Smad4 would drive a higher level of Snail transcription. Supporting this explanation, knocking down either Smad3 or Smad4 abrogated Smad2 loss–associated Snail overexpression, and a previous study showed that the combination of Smad3 and Smad4 had the highest transcriptional activity on the Snail promoter (9). Our data also helps to explain the difference between our current finding and a previous finding showing that a dominant-negative form of either Smad2 or Smad3 blocked TGF-β1–induced EMT in skin SCC cells (8). In that study, either increased Smad4 binding to the Snail promoter or the loss of corepressors should not occur due to the presence of WT Smad2. Since *Smad4*$^{-/-}$ skin and early stage SCCs did not undergo EMT or exhibit the associated molecular alterations even in the presence of Smad2 and Smad3, Smad4 appears to be indispensable for EMT at least at early stages of skin carcinogenesis. Similar to our current finding, a previous study shows that pancreatic ductal adenocarcinomas derived from *Smad4*-null cells are more well differentiated and have less EMT in comparison with tumors with intact Smad4 (37). Consistently, Ju et al. (19) reported that in hepatocyte-specific *Smad2*-knockout mice, hepatocytes underwent de-differentiation and EMT, whereas *Smad3*$^{-/-}$ hepatocytes did not. Since Smad4 was not lost in *Smad2*$^{-/-}$ skin and in early stage tumor cells, enhanced Smad4 binding to the Snail promoter is likely the major contributor to increased Snail expression, at least at early stages of skin carcinogenesis in *Smad2*$^{-/-}$ mice. When Smad4 is lost at late stages, multiple genetic/epigenetic alterations accumulated in tumor epithelia could be sufficient to sustain EMT and invasion. To this end, other pathways commonly activated in late-stage skin carcinogenesis, e.g., AKT and NF-κB, have been shown to activate Snail expression and EMT (38, 39).

It is worthwhile to mention that accelerated EMT does not always contribute to malignant progression. For instance, *Smad4*$^{-/-}$ keratinocytes did not exhibit EMT but proceeded to become spontaneous SCCs (13, 14). Conversely, accelerated EMT in *Smad2*$^{-/-}$ keratinocytes was insufficient to cause spontaneous skin cancer formation. Thus, EMT would promote tumor invasion in vivo only when coupled with other oncogenic events. Further, all of the EMT-associated genes upregulated in *K5.Smad2*$^{-/-}$ tumors also have additional functions for promoting cancer invasion. For instance, Snail and Slug regulate cell survival and apoptosis (40–44), and Snail overexpression in the epidermis causes keratinocyte hyperproliferation (45). Tenascin C has been implicated in

angiogenesis (46). All these functions could contribute to accelerated tumor formation and progression *K5.Smad2*$^{-/-}$ mice.

In summary, we report that Smad2 and Smad4 are frequently lost in human skin SCCs. The LOH of *Smad2* and *Smad4* in human skin SCCs and the haploid insufficiency of *Smad2* and *Smad4* in mouse skin carcinogenesis (see also ref. 47) suggest that in human skin cancer, even if cancer lesions lose 1 allele of the *Smad2* or *Smad4* or reduce their proteins to less than 50%, these lesions may have lost the tumor suppressive effect of Smad2 or Smad4. On the other hand, our study also shows that Smad2 loss–associated increase in Smad4 binding to the Snail promoter beyond a physiological level facilitates Snail activation and EMT. Our study prompts future research into how loss of both Smad2 and Smad4 affects skin carcinogenesis in vivo. It also remains to be determined how Smad2 loss after tumor formation, as seen in human cancers, affects tumor differentiation and malignant progression.

Methods

Human skin SCC collection and sample preparation. Human skin SCC and normal skin samples were from a human SCC tissue array (US Biomax) and were collected from surgically resected specimens between the years 2000 and 2005 from consenting patients at Oregon Health & Science University under an Institutional Review Board–approved protocol. The tissue array contained 75 SCCs and 4 normal skin samples graded by 2 pathologists from the vendor. We confirmed the grade for samples from both the tissue array and the ones we collected. In total, tissues used for IHC included 83 SCC cases and 10 normal skin samples. Tissues used for immunofluorescence included 75 SCC cases and 4 skin samples. Tissues used for quantitative RT-PCR (qRT-PCR) assays included 33 poorly differentiated skin SCCs and 6 normal skin samples. Among these, 21 samples that contained adjacent nonneoplastic skin in paraffin sections were microscopically dissected, and tissues scrapings from nonneoplastic skin and SCCs were collected separately. For LOH analysis, DNA from these tissue sections was extracted using the WaxFree DNA Paraffin Sample DNA extraction kit (TrimGen Inc.) and used for PCR, using primers for microsatellite repeat regions (48) (D18S555, forward 5′-FAM-GTGCGATGGCAAAATAGATG-3′, reverse 5′-ATTTTCTAGGAAAGAGC-TAGC-3′; D18S1137, forward 5′-FAM-TGACTATTTGCACATCTGGC-3′, reverse 5′-GGACTTGCACGCTAATGAC-3′; D18S460, forward 5′-FAM-CTGAAGGGTCCTTGCC-3′, reverse 5′-GCCAGCCTTGGCAGTC-3′). PCR products were column purified (Wizard SV Gel and PCR Clean-Up System; Promega) and analyzed using fragment length polymorphism analysis (Applied Biosystems 3130xL and Peak Scanner Software, version 1.0). LOH was determined using the following formula: peak height of allele 1 of tumor divided by peak height of allele 2 of tumor, the result of which was divided by peak height of allele 1 of adjacent skin divided by peak height of allele 2 of adjacent skin, the result of which was greater than 1.5.

Tissue histology, tumor classification, and IHC. Skin and tumor samples were fixed in 10% neutral-buffered formalin at 4°C overnight, embedded in paraffin, sectioned to 6 μm thickness, and stained with H&E. Tumor types were determined by H&E analysis, using the criteria described previously (49). IHC was performed on paraffin sections as we have previously described (25), using primary antibodies against human and mouse Smad2 (1:200; Zymed), Smad3 (1:100; Santa Cruz Biotechnology Inc.), and Smad4 (1:100; Santa Cruz Biotechnology Inc.). Sections were counterstained with hematoxylin.

Generation of inducible and keratinocyte-specific Smad2- and Smad4-knockout mice. The *K5.Cre*PR1*, the *Smad2*$^{f/f}$ line, and *Smad4*$^{f/f}$ line were generated on a C57BL/6 background as previously reported (18, 19, 50). *K5.Cre*PR1* mice were crossed with *Smad2*$^{f/f}$ or *Smad4*$^{f/f}$ mice to generate WT, *K5.Smad2*$^{f/wt}$, *K5.Smad2*$^{f/f}$, or *K5.Smad4*$^{f/f}$ genotypes. For genotyping, PCR using tail DNA was performed with primers specific for the floxed region and the Cre recombinase as previously reported (18, 19, 50). Cre-mediated *Smad2* or *Smad4* deletion in keratinocytes was achieved with topical application of RU486 (20 μg in 100 μl ethanol) once a day for 3–5 days at time points specified in the Results section. *Smad2* or *Smad4* gene deletion was detected by PCR performed on DNA extracted from RU486-treated skin, using deletion-specific primers (19, 50).

Skin chemical carcinogenesis protocol. Eight-week-old mouse skin was shaved and topically treated with 20 μg of DMBA (dissolved in 50 μl acetone; Sigma-Aldrich). One week later, 5 μg of TPA (dissolved in 50 μl acetone; Sigma-Aldrich) was applied to skin twice a week for 20 weeks. In total, 20 *Smad2*$^{+/+}$, 19 *Smad2*$^{-/-}$, and 12 *Smad2*$^{+/-}$ mice, with equal distribution of genders in each group, were used in the carcinogenesis study (17).

RNA extraction and qRT-PCR. RNA was isolated from human and mouse skin and tumors using RNAzol B (Tel-Test), as we have previously described (51), and purified using a QIAGEN RNeasy Mini kit (QIAGEN). The qRT-PCR was performed as we have previously described (52). Transcripts of human Smad2 and Smad4, mouse Smad2, K8, Snail, Slug, vimentin, tenascin C, and E-cadherin were examined using corresponding Taqman Assays-on-Demand probes (Applied Biosystems). A K14 or GAPDH RNA probe was used as an internal control. Three to nine samples from each genotype of mice or cultured cells were used for qRT-PCR. The mean expression level from *K5.Smad2*$^{+/+}$ samples (unless otherwise specified) of each particular gene being analyzed was set as 1 arbitrary unit.

Double-stain immunofluorescence. Double-stain immunofluorescence on paraffin-embedded tissue sections was performed as we have previously described (53). Each section was incubated overnight at 4°C with a primary antibody together with a guinea pig antiserum against mouse K14, the latter of which highlights the epithelial compartment of the skin (51). An Alexa Fluor 488–conjugated (green) secondary antibody against the species of the primary antibody (1:100–1:400; Molecular Probes) and Alexa Fluor 594–conjugated (red) anti–guinea pig secondary antibody (1:100; Molecular Probes) were used to visualize the staining. The primary antibodies included K1 (1:500; Covance), K8 (1:100; Fitzgerald), vimentin (1:200; Sigma-Aldrich), E-cadherin (1:100; BD Bioscience), K14 (1:400; Fitzgerald), Snail (1:200; Abcam), and αSMA (1:200; Sigma-Aldrich).

Quantitative chromatin immunoprecipitation. Four mouse back skins from each group of WT and *K5.Smad2*$^{-/-}$ mice were homogenized on ice in 5 ml of 1% formalin and incubated at room temperature for 30 minutes after adding an additional 5 ml of 1% formalin to each tube. Each sample was then diluted in 1 ml of 10X Glycine Stop Solution (Active Motif), incubated at room temperature for 5 minutes, and then centrifuged at 1,400 *g* for 10 minutes at 4°C. The resulting pellet was used for ChIP Enzymatic Digestion following the manufacturer's protocol (Active Motif). Antibodies, 3 μg/each, to Smad2 (Zymed), Smad3 (Upstate), and Smad4 (Upstate) were used to immunoprecipitate the sheared chromatin complexes. Rabbit IgG (3 μg; Santa Cruz Biotechnology Inc.) was used as a negative control for antibody specificity. DNA obtained from eluted beads was used for quantitative PCR using Power SYBR Green Master Mix (Applied Biosystems). Primers encompassing the SBE sites of the Snail promoter (Supplemental Table 1) were used for PCR. Positive binding was defined as antibody binding more than 10-fold of the IgG-negative control. Difference in Ct (ΔCt) values were obtained by normalizing IP Ct values to input values for each group. ΔΔCt values were obtained by comparing the ΔCt values of *Smad2*$^{-/-}$ skin to WT skin. Values are expressed as fold change based on ΔΔCt values.

HaCaT keratinocyte culture and siRNA knockdown. HaCaT keratinocytes were cultured in DMEM with high levels of glucose with 10% FBS and penicillin-streptomycin antibiotics. Twenty-four hours prior to siRNA transfection, cells were switched to DMEM with low levels of glucose with

0.2% FBS and penicillin-streptomycin antibiotics. Cells were transfected with siRNAs for human Smad2, Smad3, Smad4, or Snail (Supplemental Table 2) using XtremeGene siRNA Transfection Reagent (Roche) in 6-well plates or chamber slides, at a final concentration of 50 pmol siRNA/μl in Optimem media (Gibco). Four hours posttransfection, media was switched to DMEM with high levels of glucose. Prior to cell harvest in culture dishes or fixation in the chamber slides, cells were treated with or without 10 pM TGF-β1 for period of times specified in the Results section. Cells were harvested at 48 or 72 hours after siRNA transfection for RNA extraction using Qiashredder and RNeasy kits (QIAGEN). Chamber slides were fixed for 40 minutes at room temperature in 2% paraformaldehyde and stained with antibodies specified in the Results section, using the methods as described above.

Statistics. Significant differences between the values obtained in each assay on samples from various genotypes were determined using the Student's *t* test and expressed as mean ± SEM, with the exception of evaluation of human SCCs and tumor malignancy, in which a χ^2 test was used. *P* values of less than 0.05 were considered significant.

Acknowledgments

The authors thank Qinghong Zhang and Jiri Zavadil for suggestions for the experiments. We would also like to thank an anonymous donation to our research related to this publication. This work was supported by NIH grants to X.-J. Wang. K.E. Hoot and J. Lighthall are recipients of NIH training grants.

Received for publication October 15, 2007, and accepted in revised form May 28, 2008.

Address correspondence to: Xiao-Jing Wang, Portland VA Cancer Center (R&D 46), Building 103, Room F-221, 3710 SW US Veterans Hospital Road, Portland, Oregon 97239-2999, USA. Phone: (503) 220-8262, ext. 54273; Fax: (503) 402-2817; E-mail: wangxiao@ohsu.edu.

Xiao-Jing Wang's present address is: Portland VA Cancer Center, Portland, Oregon, USA.

1. Massagué, J., Seoane, J., and Wotton, D. 2005. Smad transcription factors. *Genes Dev.* **19**:2783–2810.
2. Massague, J., and Gomis, R.R. 2006. The logic of TGFbeta signaling. *FEBS Lett.* **580**:2811–2820.
3. Brown, K.A., Pietenpol, J.A., and Moses, H.L. 2007. A tale of two proteins: differential roles and regulation of Smad2 and Smad3 in TGFβ signaling. *J. Cell. Biochem.* **101**:9–33.
4. Nomura, M., and Li, E. 1998. Smad2 role in mesoderm formation, left-right patterning and craniofacial development. *Nature.* **393**:786–790.
5. Yang, X., Li, C., Xu, X., and Deng, C. 1998. The tumor suppressor SMAD4/DPC4 is essential for epiblast proliferation and mesoderm induction in mice. *Proc. Natl. Acad. Sci. U. S. A.* **95**:3667–3672.
6. Yang, X., et al. 1999. Targeted disruption of SMAD3 results in impaired mucosal immunity and diminished T cell responsiveness to TGF-beta. *EMBO J.* **18**:1280–1291.
7. Bierie, B., and Moses, H.L. 2006. TGFbeta: the molecular Jekyll and Hyde of cancer. *Nat. Rev. Cancer.* **6**:506–520.
8. Oft, M., Akhurst, R.J., and Balmain, A. 2002. Metastasis is driven by sequential elevation of H-ras and Smad2 levels. *Nat. Cell Biol.* **4**:487–494.
9. Cho, H.J., Baek, K.E., Saika, S., Jeong, M.J., and Yoo, J. 2007. Snail is require for transforming growth factor-beta-induced epithelial-mesenchymal transition by activating PI3 kinase/Akt signal pathway. *Biochem. Biophys. Res. Commun.* **353**:337–343.
10. Ten Dijke, P., Goumans, M.J., Itoh, F., and Itoh, S. 2002. Regulation of cell proliferation by Smad proteins. *J Cell. Physiol* **191**:1–16.
11. Sjoblom, T., et al. 2006. The consensus coding sequences of human breast and colorectal cancers. *Science.* **314**:268–274.
12. Wolfraim, L.A., et al. 2004. Loss of Smad3 in acute T-cell lymphoblastic leukemia. *N. Engl. J. Med.* **351**:552–559.
13. Yang, L., et al. 2005. Targeted disruption of Smad4 in mouse epidermis results in failure of hair follicle cycling and formation of skin tumors. *Cancer Res.* **65**:8671–8678.
14. Qiao, W., et al. 2006. Hair follicle defects and squamous cell carcinoma formation in Smad4 conditional knockout mouse skin. *Oncogene.* **25**:207–217.
15. Vijayachandra, K., Lee, J., and Glick, A.B. 2003. Smad3 regulates senescence and malignant conversion in a mouse multistage skin carcinogenesis model. *Cancer Res.* **63**:3447–3452.
16. Tannehill-Gregg, S.H., Kusewitt, D.F., Rosol, T.J., and Weinstein, M. 2004. The roles of Smad2 and Smad3 in the development of chemically induced skin tumors in mice. *Vet. Pathol.* **41**:278–282.
17. Li, A.G., Lu, S.L., Zhang, M.X., Deng, C., and Wang, X.J. 2004. Smad3 knockout mice exhibit a resistance to skin chemical carcinogenesis. *Cancer Res.* **64**:7836–7845.
18. Caulin, C., et al. 2004. Inducible activation of oncogenic K-ras results in tumor formation in the oral cavity. *Cancer Res.* **64**:5054–5058.
19. Ju, W., et al. 2006. Deletion of Smad2 in mouse liver reveals novel functions in hepatocyte growth and differentiation. *Mol. Cell. Biol.* **26**:654–667.
20. Rugg, E.L., and Leigh, I.M. 2004. The keratins and their disorders. *Am. J. Med. Genet. C Semin. Med. Genet.* **131C**:4–11.
21. Huber, M.A., Kraut, N., and Beug, H. 2005. Molecular requirements for epithelial-mesenchymal transition during tumor progression. *Curr. Opin. Cell Biol.* **17**:548–558.
22. Hendrix, M.J., Seftor, E.A., Seftor, R.E., and Trevor, K.T. 1997. Experimental co-expression of vimentin and keratin intermediate filaments in human breast cancer cells results in phenotypic interconversion and increased invasive behavior. *Am. J. Pathol.* **150**:483–495.
23. Masszi, A., et al. 2003. Central role for Rho in TGF-beta1-induced alpha-smooth muscle actin expression during epithelial-mesenchymal transition. *Am. J. Physiol. Renal Physiol.* **284**:F911–F924.
24. Zavadil, J., and Bottinger, E.P. 2005. TGFbeta and epithelial-to-mesenchymal transitions. *Oncogene.* **24**:5764–6774.
25. Han, G., et al. 2005. Distinct mechanisms of TGF-β1–mediated epithelial-to-mesenchymal transition and metastasis during skin carcinogenesis. *J. Clin. Invest.* **115**:1714–1723.
26. He, W., Cao, T., Smith, D.A., Myers, T.E., and Wang, X.J. 2001. Smads mediate signaling of the TGFbeta superfamily in normal keratinocytes but are lost during skin chemical carcinogenesis. *Oncogene.* **20**:471–483.
27. Peinado, H., Quintanilla, M., and Cano, A. 2003. Transforming growth factor beta-1 induces snail transcription factor in epithelial cell lines. *J. Biol. Chem.* **278**:21113–21123.
28. Lüttges, J., et al. 2001. Allelic loss is often the first hit in the biallelic inactivation of the p53 and DPC4 genes during pancreatic carcinogenesis. *Am. J. Pathol.* **158**:1677–1683.
29. Kavsak, P., et al. 2000. Smad7 binds to Smurf2 to form an E3 ubiquitin ligase that targets the TGFβ receptor for degradation. *Mol. Cell.* **6**:1365–1375.
30. Lin, X., Liang, M., and Feng, X.H. 2000. Smurf2 is a ubiquitin E3 ligase mediating proteasome-dependent degradation of Smad2 in transforming growth factor-beta signaling. *J. Biol. Chem.* **275**:36818–36822.
31. Wan, M., et al. 2004. Smad4 protein stability is regulated by ubiquitin ligase SCF beta-TrCP1. *J. Biol. Chem.* **279**:14484–14487.
32. Liang, M., et al. 2004. Ubiquitination and proteolysis of cancer-derived Smad4 mutants by SCFSkp2. *Mol. Cell. Biol.* **24**:7524–7537.
33. Dlugosz, A., Merlino, G., and Yuspa, S.H. 2002. Progress in cutaneous cancer research. *J. Investig. Dermatol. Symp. Proc.* **7**:17–26.
34. Xie, W., et al. 2003. Frequent alterations of Smad signaling in human head and neck squamous cell carcinomas: a tissue microarray analysis. *Oncol. Res.* **14**:61–73.
35. Corominas, M., et al. 1991. ras activation in human tumors and in animal model systems. *Environ. Health Perspect.* **93**:19–25.
36. Lu, S.L., et al. 2006. Loss of transforming growth factor b type II receptor promotes metastatic head-and-neck squamous cell carcinoma. *Genes Dev.* **20**:1331–1342.
37. Bardeesy, N., et al. 2006. Smad4 is dispensable for normal pancreas development yet critical in progression and tumor biology of pancreas cancer. *Genes Dev.* **20**:3130–3146.
38. Dong, R., et al. 2007. Role of nuclear factor kappa B and reactive oxygen species in the tumor necrosis factor-α-induced epithelial-mesenchymal transition of MCF-7 cells. *Braz. J. Med. Biol. Res.* **40**:1071–1078.
39. Lester, R.D., Jo, M., Montel, V., Takimoto, S., and Gonias, S.L. 2007. uPAR induces epithelial-mesenchymal transition in hypoxic breast cancer cells. *J. Cell Biol.* **178**:425–436.
40. Zha, Y., He, J., Mei, Y., Yin, T., and Mao, L. 2007. Zinc-finger transcription factor Snail accelerates survival, migration, and expression of matrix metalloproteinase-2 in human bone mesenchymal stem cells. *Cell Biol. Int.* **31**:1089–1096.
41. Peinado, H., Olmeda, D., and Cano, A. 2007. Snail, ZEB, and bHLH factors in tumor progression: an alliance against the epithelial phenotype? *Nat. Rev. Cancer.* **7**:415–428.
42. Papadavid, E., Pignatelli, M., Zakynthinos, S., Krausz, T., and Chu, A.C. 2002. Abnormal immunoreactivity of the E-cadherin/catenin (α-, β-, and γ-) complex in premalignant and malignant nonmelanocytic skin tumours. *J. Pathol.* **196**:154–162.
43. Wu, W.S., et al. 2005. Slug antagonizes p53-mediated apoptosis of hematopoietic progenitors by repressing *puma*. *Cell.* **123**:641–653.
44. Craene, B.D., vanRoy, F., and Berx, G. 2005. Unraveling signalling cascades for the Snail family of transcription factors. *Cell Signal.* **17**:535–547.
45. Jamora, C., et al. 2005. A signaling pathway involv-

ing TGF-beta2 and snail in hair follicle morphogenesis. *PLoS Biol.* **3**:e11.
46. Ballard, V.L., et al. 2006. Vascular tenascin-C regulates cardiac endothelial phenotype and neovascularization. *FASEB J.* **20**:717–719.
47. Teng, Y., et al. 2006. Synergistic function of Smad4 and PTEN in suppressing forestomach squamous cell carcinoma in the mouse. *Cancer Res.* **66**:6972–6981.
48. Toda, T., et al. 2001. Analysis of microsatellite instability and loss of heterozygosity in uterine endometrial adenocarcinoma. *Cancer Genet. Cytogenet.* **126**:120–127.
49. Aldaz, C.M., Conti, C.J., Klein-Szanto, A.J., and Slaga, T.J. 1987. Progressive dysplasia and aneuploidy are hallmarks of mouse skin papillomas: relevance to malignancy. *Proc. Natl. Acad. Sci. U. S. A.* **84**:2029–2032.
50. Yang, X., Li, C., Herrera, P.L., and Deng, C.X. 2002. Generation of Smad4/Dpc4 conditional knockout mice. *Genesis.* **32**:80–81.
51. Wang, X.J., Greenhalgh, D.A., Lu, X.R., Bickenbach, J.R., and Roop, D.R. 1995. TGF alpha and v-fos cooperation in transgenic mouse epidermis induces aberrant keratinocyte differentiation and stable, autonomous papillomas. *Oncogene.* **10**:279–289.
52. Lu, S.L., et al. 2004. Overexpression of transforming growth factor beta1 in head and neck epithelia results in inflammation, angiogenesis, and epithelial hyperproliferation. *Cancer Res.* **64**:4405–4410.
53. Li, A.G., Wang, D., Feng, X.H., and Wang, X.J. 2004. Latent TGFbeta1 overexpression in keratinocytes results in a severe psoriasis-like skin disorder. *EMBO J.* **23**:1770–1781.